HOKKAIDO UNIVERSITY

Title	Effects of Dosage Increase on Electrical Properties of Metal-Oxide-Semiconductor Diodes with Mg-Ion-Implanted GaN Before Activation Annealing
Author(s)	Akazawa, Masamichi; Kamoshida, Ryo; Murai, Shunta et al.
Citation	Physica status solidi B-basic solid state physics, 257(2), 1900367 https://doi.org/10.1002/pssb.201900367
Issue Date	2020-02-06
Doc URL	https://hdl.handle.net/2115/80376
Rights	This is the peer reviewed version of the following article: Akazawa, M. , Kamoshida, R. , Murai, S. , Narita, T. , Omori, M. , Suda, J. and Kachi, T. (2019), Effects of Dosage Increase on Electrical Properties of Metal - Oxide - Semiconductor Diodes with Mg - Ion - Implanted GaN Before Activation Annealing. Phys. Status Solidi B. , which has been published in final form at https://doi.org/10.1002/pssb.201900367. This article may be used for non-commercial purposes in accordance with Wiley Terms and Conditions for Use of Self-Archived Versions.
Type	journal article
File Information	ssb201900367_for printing.pdf

Hokkaido University Collection of Scholarly and Academic Papers : HUSCAP

Effects of dosage increase on electrical properties of metal-oxide-semiconductor diodes with Mg-ion-implanted GaN before activation annealing

Masamichi Akazawa[1]*, *Ryo Kamoshida*[1], *Shunta Murai*[1], *Tetsuo Narita*[2], *Masato Omori*[3, [+]], *Jun Suda*[3, 4] *and Tetsu Kachi*[3]

[1]*Research Center for Integrated Quantum Electronics, Hokkaido University, Sapporo 060-0813, Japan*

[2]*Toyota Central R&D Labs., Inc., Yokomichi, Nagakute 480-1192, Japan*

[3]*Institute of Materials and Systems for Sustainability, Nagoya University, Nagoya 464-8601, Japan*

[4]*Department of Electronics, Nagoya University, Nagoya 464-8603, Japan*

[+]Present address: *Department of Innovative Engineering, Oita University, Oita 870-1192, Japan*

*E-mail: akazawa@rciqe.hokudai.ac.jp

Keywords: GaN, MOS, deep level, Mg-ion implantation

The effect of increasing the dosage on the electrical properties of Mg-ion-implanted GaN before activation annealing is investigated to obtain knowledge on the defect levels generated by ion implantation. To probe the near-surface region, GaN MOS structures with Al_2O_3 were used. Two kinds of MOS diodes with Mg-ion dosages of 1.5×10^{11} cm^{-2} and 1.5×10^{12} cm^{-2} implanted at 50 keV were prepared. Although anomalous capacitance–voltage (*C–V*) characteristics were observed for the low-dosage sample, they were improved by annealing at 600 ºC for 3 h. However, for the high-dosage sample, more severe and persistent frequency dispersion was observed in the *C–V* characteristics, which was not improved by the same annealing. On the basis of the detailed analysis of capacitance–frequency (*C–f*) characteristics, it is concluded that the discrete interface trap at 0.2–0.3 eV below the conduction band was responsible for the frequency dispersion observed for the high-dosage sample. Combined with the results of deep-level transient spectroscopy, it is highly likely that the bulk deep levels affected the *C–V* and *C–f* characteristics. The possibility that the dominant deep levels were changed by the increase in Mg-ion dosage is discussed.

1. Introduction

GaN has a high electron saturation velocity and a high breakdown voltage and can form a heterostructure with other III-nitride alloys[1]. With these features, recent attention has focused on the application of GaN to power devices[2, 3], although this material was behind the revolution in the efficiency of light-emitting diodes and has contributed to energy conservation[4, 5]. A timely report on an excellent property of an Al_2O_3/GaN on GaN interface formed by atomic layer deposition (ALD) is available[6, 7] and enhanced the applicability of GaN being expanded to power devices, *i.e.*, metal-oxide-semiconductor field effect transistors (MOSFETs). In particular, a vertical MOSFET is a useful power device for achieving a high breakdown voltage and a low on-resistance[3, 8–10]. To construct power devices, including vertical MOSFETs, ion implantation is a convenient method of obtaining a selectively doped region. Although the formation of the n-type region can be practically accomplished by Si-ion implantation, that of the p-type region has been difficult by ion implantation. Although the most promising method for implanting acceptors is Mg-ion implantation, satisfactory doping control of Mg acceptors is difficult to achieve.

Recently, attempts have been made to achieve sufficient activation of implanted Mg acceptors[11–18]. Commonly, activation is achieved by thermal annealing at a temperature higher than 1,200 ºC or, more specifically, 1,230 ºC[15, 16]. The activation ratio should be defined as the ratio of the hole concentration to the acceptor density. Owing to an activation energy as high as 160 meV[19–21], the activation ratio decreases with increasing doping density of acceptors. Using symmetric multicycle rapid thermal annealing (SMRTA) in nitrogen overpressure, an activation ratio as high as 10%[14] has been achieved, which agrees with the theoretical limit. However, the highest activation ratio of 2.3%[18] achieved by conventional RTA is lower than the theoretical limit. In consideration of mass production, an efficient annealing method in an ordinary furnace must be established. For this purpose, defects generated by Mg-ion implantation should be investigated to find a control method.

Ion implantation can generate vacancies of gallium V_{Ga} and nitrogen V_N. The results of positron annihilation spectroscopy (PAS) in the study of Mg-ion-implanted GaN[22, 23] showed that the divacancy V_{Ga}–V_N is mainly generated by implantation at room temperature and that the agglomeration to form larger vacancy clusters proceeds upon annealing at 1,000 ºC. These vacancy clusters still existed even after annealing at 1,300 ºC. Nevertheless, a new clue to control the defects generated by Mg-ion implantation might be found by applying low-temperature annealing. Recently, it was reported that annealing at 800 ºC for 3 min after Mg-ion implantation reduced the density of the deep-level states in lightly Mg-ion-implanted

GaN[24]. A detailed deep-level transient spectroscopy (DLTS) study has been conducted to investigate the effect of low-temperature annealing for 1 min on defects generated by Mg-ion implantation at a low dosage[25]. Very recently, the effect of low-temperature annealing was also monitored using MOS diodes with Mg-ion implanted GaN for the case of relatively low dosage, to find that 500–700 ºC annealing for 3 min was efficient to improve the electrical properties of ion-implanted GaN[26]. However, these electrical measurements were performed on low-dosage GaN samples. The effect of increasing the dosage has not been investigated. In this work, we studied the effects of increasing the dosage on the electrical properties of MOS diodes with Mg-ion-implanted GaN before activation annealing.

2. Experimental procedure

In this work, GaN MOS structures with Al_2O_3 were used to investigate the near-surface region of Mg-ion-implanted GaN. The sequence of sample preparation is shown in **Figure 1**. A 3-μm-thick n-type GaN layer ($n = 5\times10^{17}$ cm^{-3}) was grown on a freestanding c-plane n^+-GaN substrate (the dislocation density of the freestanding substrate was lower than 5.0×10^6 cm^{-2}) by metalorganic vapor phase epitaxy. Mg-ion implantation was carried out with an energy of 50 keV and an angle of 7º at room temperature. A sample with a dosage of 1.5×10^{11} cm^{-2} and another with a dosage of 1.5×10^{12} cm^{-2} were prepared. **Figure 2** is a plot of the Mg density profile obtained by the TRIM simulation in the full cascade calculation mode with displacement energies of 28 eV and 25 eV for N and Ga, respectively. For samples with long-term 600 ºC annealing, a 20-nm-thick Al_2O_3 layer was deposited by ALD at 300 ºC using H_2O and trimethylaluminum, followed by annealing at 600 ºC for 3 h in nitrogen flow and subsequent removal of the Al_2O_3 layer using a solution of HF:NH_4F = 1:5. A MOS diode structure was fabricated by depositing 30-nm-thick ALD Al_2O_3 and forming Ni/Au top electrodes and a Ti/Au back ohmic contact. After completion of the MOS diodes, post-metallization annealing (PMA) was carried out to reduce the density of interface states at the Al_2O_3/GaN interface. For comparison, samples without long-term 600 ºC annealing and a sample with as-grown GaN without Mg-ion implantation were also prepared.

The capacitance–voltage (*C–V*) and capacitance–frequency (*C–f*) measurements at frequencies ranging from 1 kHz to 1 MHz and the current density–voltage (*J–V*) measurement were performed at room temperature. The bias sweep rate in the *C–V* measurement was 50 mV/s. DLTS was also carried out in the temperature range of 40–560 K for the same MOS diodes. Since the dosage of Mg ions is relatively low here, there is a possibility that popular structural and chemical analysis methods such as atomic force microscopy, X-ray diffraction,

and X-ray photoelectron spectroscopy may not reveal the effect of Mg-ion implantation. Nevertheless, electrical measurements make it possible to investigate the effect of low-dosage Mg-ion implantation in GaN. Therefore, we concentrated on the electrical measurements. An investigation of a sample with a much higher dosage is beyond the scope of this paper.

3. Results and discussion

3.1. *J–V* and *C–V* characteristics

The measured *J–V* characteristics are summarized and compared in **Figure 3** for all of the fabricated MOS diodes. Relatively low *J* was obtained in the entire applied voltage range for each sample. This result indicates that every MOS diode can be used for the *C–V* measurement without any adverse effect of the leakage current. Lower *J* for the high-dosage samples in the plus bias region may result from deep depletion, while higher *J* for the as-grown and the low-dosage samples may indicate the achievement of surface accumulation in the same bias region. These expectations were confirmed by the *C–V* measurement as described in the following.

Figure 4(a) shows the *C–V* characteristics measured for the MOS diode with as-grown GaN without Mg-ion implantation. The *C–V* curves almost overlap the ideal one assuming no interface states. In addition, the frequency dispersion and the hysteresis are negligible. This result indicates that the interface state density was extremely low at the Al_2O_3/GaN interface and that bulk deep levels with concentrations sufficient to affect the *C–V* characteristics did not exist in the as-grown GaN epitaxial layer. Figure 4(b) shows the *C–f* characteristics measured for the same sample. As is expected from the *C–V* characteristics, flat capacitance curves can be seen. These results are starting points for investigating the *C–V* and *C–f* characteristics.

The *C–V* characteristics measured for the sample with the lower dosage are shown in **Figure 5**, where the ideal curve is the theoretical curve assuming no interface states for the MOS diode with the as-grown GaN without Mg-ion implantation. Without long-term 600 ºC annealing, the *C–V* curves show anomalous shapes compared with the ideal curve, as shown in Figure 5(a). The plateau region and anomalously steep region indicate the existence of an acceptor-type discrete state in the band gap, as discussed in detail in the previous work[24, 26]. Note that the anomalous behavior was much improved by long-term 600 ºC annealing, as shown in Figure 5(b), where the hysteresis and frequency dispersion are minimized without showing a plateau region. This result shows that the dominant defect level was greatly reduced by long-term 600 ºC annealing. In the previous work[26], although annealing at 400 ºC for 3 min was applied to the low-dosage sample made by the same process sequence including ALD and the removal of Al_2O_3, the *C–V* characteristics were not improved. Therefore, ALD and the removal

of Al_2O_3 before and after long-term 600 °C annealing of the present sample do not improve the discrete state.

The *C–V* characteristics were changed by increasing the dosage by one order and the effect of annealing was less marked for the high-dosage sample. **Figure 6**(a) shows the *C–V* characteristics for the high-dosage sample without long-term 600 °C annealing. Severe frequency dispersion can be seen in the relatively high frequency range of 1 kHz to 1 MHz. This behavior was not significantly improved by long-term 600 °C annealing, as shown in Figure 6(b). The difference between the capacitances measured at 100 kHz and 1 MHz is the widest among the measured frequencies, which suggests the existence of a deep level at an energy level near the conduction band edge E_C. On the other hand, the considerable hysteresis in both Figure 6(a) and 6(b) indicates the existence of another deep level with a longer time constant or a deeper energy position. Although we have not performed higher temperature annealing, we consider it a future work.

As was discussed in the previous work[26], the *C–V* characteristics for the low-dosage samples can be explained by the existence of a deep level at E_C – 0.7 eV. However, this energy level has a time constant τ of 8.6 – 860 s if we assume the capture cross section σ to be 1×10^{-17} – 1×10^{-15} cm^2 in the equation given by[25, 27, 28]

$$\tau = \frac{1}{\sigma v_{th} N_C} exp\left(\frac{E_C - E_T}{kT}\right), \quad (1)$$

where v_{th} is the electron thermal velocity, N_C is the effective density of states at the conduction band bottom, E_T is the energy of the deep level, k is the Boltzmann constant, and T is the temperature. Therefore, the existence of the deep level at E_C – 0.7 eV cannot explain the observed frequency dispersion for the high-dosage sample, although it well explains the behavior of the hysteresis for both samples. This implies the existence of a shallower deep level in the high dosage sample. Nevertheless, there is also a possibility that the interface states caused the frequency dispersion. To distinguish this, *C–f* measurement was carried out as described in the following subsection.

3.2. Analysis of *C–f* characteristics

The *C–f* characteristics measured for the high-dosage sample without long-term 600 °C annealing are shown in **Figure 7**(a). It can be seen that the frequency dependent *C–f* curve shifts with the bias. However, the relaxation frequency of each *C–f* curve with the conductance, G/ω, peak seems to saturate as the bias voltage increases. As shown in Figure 5(b), a slight change

in the *C*–*f* characteristics was observed for the high-dosage sample with long-term 600 °C annealing. Nevertheless, the behavior of the relaxation frequency is similar to the case without long-term 600 °C annealing, indicating saturation with increasing bias.

The observed frequency dispersion is likely caused by interface traps. To investigate the time constant of the interface traps, let us transform the equivalent circuit for measured data to that for the physical model of the MOS diode. **Figure 8**(a) shows the equivalent circuit used in the *C*–*V* and *C*–*f* measurements consisting of the measured capacitance C_m and conductance G_m, while Figure 8(b) indicates that for the physical model of a MOS diode with oxide capacitance C_{OX}, depletion layer capacitance C_D, and the interface trap admittance consisting of frequency dependent capacitance C_p and frequency dependent conductance G_p. Here, C_p and G_p can be calculated by[29–31]

$$C_p = \frac{\left\{(C_{OX}-C_m)C_m-\left(G_m/\omega\right)^2\right\}C_{OX}}{\left(G_m/\omega\right)^2+(C_{OX}-C_m)^2} - C_D \tag{2}$$

and

$$\frac{G_p}{\omega} = \frac{C_{OX}^2\left(G_m/\omega\right)}{\left(G_m/\omega\right)^2+(C_{OX}-C_m)^2}. \tag{3}$$

According to the results of the calculation using these equations, G_p/ω–C_p diagrams, referred to as "Cole–Cole diagrams"[32, 33] are plotted in **Figure 9** where the solid circles indicate the experimental data and solid lines indicate fitting lines assuming a single time constant. If the time constant of the interface traps is single, the equivalent circuit for the interface trap admittance can be drawn by a series connection of a frequency independent capacitance, C_{it}, and a frequency independent resistance, R_{it}, both of which are constants. For this case, C_p and G_p/ω can be given by

$$C_p = \frac{1}{1+\omega^2\tau^2}C_{it} \tag{4}$$

and

$$\frac{G_p}{\omega} = \frac{\omega\tau}{1+\omega^2\tau^2}C_{it}, \tag{5}$$

where $\tau = C_{it}R_{it}$. These equations indicate that a G_p/ω–C_p diagram should be a semicircle, as given by

$$\left(C_p - \frac{C_{it}}{2}\right)^2 + \left(\frac{G_p}{\omega}\right)^2 = \left(\frac{C_{it}}{2}\right)^2. \quad (6)$$

In Figure 9, the fitting lines are semicircles calculated using Equation (6). It can be seen that the experimental data are well fitted to the calculated semicircles, especially for the high-dosage sample without long-term 600 ºC annealing. Generally, Cole–Cole diagrams for the interface trap admittance of MOS diodes have distorted shapes far from a semicircle because of the distribution of the time constant resulting from the continuous distribution of the interface traps[33]. Therefore, it is highly likely that each measured interface trap admittance mainly results from a discrete deep level with a single time constant. The discrepancy from the semicircles at the right side, that is, the low-frequency side, indicates the existence of deeper levels, although further investigation is limited by the low-frequency limit of the measurement system. C_{it} and τ can be obtained by fitting the experimental G_p/ω–f plot to Equation (5), which leads to the extraction of interface trap density D_{it} as[31]

$$D_{it} = \frac{C_{it}}{q^2}. \quad (7)$$

The experimentally extracted G_p/ω–f plots are shown in **Figure 10**(a) for the high-dosage sample without 600 ºC annealing and in Figure 10(b) for the high-dosage sample with 600 ºC annealing. In these figures, the experimental data (solid circles) are well fitted to the theoretical curves calculated by Equation (5). The energy position of the interface traps can be obtained from τ at the peak frequency using Equation (1). If we assume σ to be 1×10^{-17} cm^2, 1×10^{-16} cm^2, and 1×10^{-15} cm^2, we can plot D_{it} as a function of the energy position, as shown in **Figure 11**. The extracted D_{it} distribution clearly indicates the existence of a discrete trap around $E_C - E$ = 0.2 – 0.3 eV. This type of D_{it} distribution is unusual. According to the disorder-induced gap state model[34, 35], interface disorder is the origin of the interface states with a U-shaped continuous D_{it} distribution consisting of the tails from the conduction and valence bands resulting from the incomplete separation of these bands. Actually, U-shaped D_{it} distribution has been measured for insulator/GaN interfaces[6]. Therefore, the detected discrete interface trap should have resulted from the bulk deep level generated by Mg-ion implantation in GaN.

3.3. Investigation of bulk deep levels

To confirm the existence of the bulk deep levels, DLTS was performed for the fabricated MOS diodes without 600 ºC annealing. The applied reverse voltage and the maximum voltage during the filling pulse were –10 V and 1 V for the as-grown sample, –5 V and –2 V for the low-dosage sample, and 0 V and 2 V for the high-dosage sample, respectively. For the GaN-on-GaN MOS diode with ALD Al_2O_3 treated by PMA, the stress-dependent flat band voltage shift was reported to be negligible, even after bias stress at 5 V, in Ref. 6. Considering the maximum voltage during the filling pulse was 2 V here, the flat band voltage shift should have been negligible. The obtained DLTS signals are shown in **Figure 12**(a) for the low-dosage sample and in Figure 12(b) for the high-dosage sample. It can be seen that the increase in dosage led to an increase in the signal intensity of level A. Level B was detected for the low-dosage sample, while level C was detected for the high-dosage sample. Arrhenius plots are summarized in **Figure 13** where the result for the as-grown n-GaN layer without implantation is also shown and the dashed lines were taken from the previous reports as reference data. Level A was either undetected or under the detection limit for the as-grown sample. The level detected for the as-grown sample can be identified as E3 in Ref. 36. Deep level B at E_C – 0.83 eV with σ of 1.8×10^{-15} cm^2 detected for the low-dosage sample is clearly different from the E3 level detected for the as-grown sample, indicating that another level was generated by Mg-ion implantation. This result is in good agreement with the previous report[25]. In addition, this energy level is close to that derived by the simulation of *C–V* characteristics of the low-dosage sample in the previous works[24, 26]. The energy position and σ of level A were E_C – 0.18 eV and 4.5×10^{-17} cm^2 for the low-dosage sample, while they were E_C – 0.19 eV and 8.0×10^{-17} cm^2 for the high-dosage sample, respectively. On the basis of the Arrhenius plot, this level is probably the E1 level in Ref. 36 rather than V_N[37]. The Arrhenius plot of deep level C at E_C – 0.51 eV with σ of 4.8×10^{-17} cm^2 is close to the E3 level, which may be identified as E3. However, since σ of deep level C is much smaller than that of E3 (1.1×10^{-15} cm^2), the possibility that level C was generated by Mg-ion implantation cannot be denied.

For the high-dosage sample, the deep level at E_C – 0.2 to E_C – 0.3 eV was derived from the *C–f* measurement. As the dosage increased, the dominance of this deep level became more marked in the *C–f* characteristics, while the DLTS signal of deep level A became more intense. Therefore, the discrete level detected by the *C–f* measurement is likely to be identified as level A. The origin of level A can be assigned to the divacancy V_{Ga}–V_N[36, 38–40]. According to the PAS results, the divacancy is the dominant defect in as-implanted GaN, which is in good agreement

with the present result for the high-dosage sample. On the other hand, for the low-dosage sample, the dominant deep level, B, was detected at E_C – 0.83 eV, which is also in good agreement with the previous reports[24–26]. In Ref. 26, a possible mechanism was discussed, in which V_{Ga} and V_N exist separately in the low-dosage sample, while the divacancy is mainly formed in a sample with a higher dosage. However, the Arrhenius plots in Figure 13 indicate that level B detected for the low-dosage sample is different from E3 that can be assigned to the nitrogen antisite N_{Ga} or V_{Ga}[36, 40, 41]. Therefore, level B should be assigned to a deeper level, *e.g.,* nitrogen interstitial N_i acceptor[41]. It is reported that N_i is annealed at 400 ºC[42], which does not contradict the present result. Therefore there is the possibility that the dominant defect changed depending on the dosage.

4. Conclusions

The effect of the dosage on the electrical properties of Mg-ion-implanted GaN was investigated using MOS diodes to obtain knowledge on the defect levels generated by ion implantation. Although anomalous *C–V* characteristics were observed for the low-dosage (1.5×10^{11} cm^{-2}) sample, they were improved by 600 ºC annealing for 3 h. However, for the high-dosage (1.5×10^{12} cm^{-2}) sample, more sever and persistent frequency dispersion was observed in the *C–V* characteristics, which was not improved by the same annealing. On the basis of the detailed analysis of *C–f* characteristics, a discrete level with a single time constant was detected. Considering the possible range of the capture cross section, it was concluded that the discrete interface traps at 0.2–0.3 eV below E_C were responsible for the frequency dispersion observed for the high-dosage sample. Combined with the results of DLTS, it is highly likely that the bulk deep level affected the *C–V* and *C–f* characteristics because a similar deep level was detected. In addition, a deep level at E_C – 0.83 eV, generated by Mg-ion implantation, was detected for the low-dosage sample. This energy level is close to that derived by the simulation of the *C–V* characteristics of the low-dosage sample in the previous works[24, 26]. Although this deep level was not detected for the high-dosage sample, a deep level at E_C – 0.51 eV was detected. The origin of the detected deep levels was discussed.

Acknowledgments

This research is supported by the Ministry of Education, Culture, Sports, Science and Technology (MEXT), Japan, through its “Program for research and development of next-generation semiconductor to realize energy-saving society.”

Conflict of Interest

The authors declare no conflict of interest.

References

[1] D. Ueda, in *Power GaN Devices* (Eds: M. Meneghini, G. Meneghesso, and E. Zanoni), Springer, New York, NY **2017**, Ch. 1.

[2] T. Kachi, *Jpn. J. Appl. Phys.* **2014**, 53, 100210.

[3] H. Amano, Y Baines, E. Beam, M. Borga, T. Bouchet, P. R Chalker, M. Charles, K. J. Chen, N. Chowdhury, R. Chu, C. De Santi, M. M. De Souza, S. Decoutere, L. Di Cioccio, B. Eckardt, T. Egawa, P. Fay, J. J. Freedsman, L. Guido, O. Häberlen, G. Haynes, T. Heckel, D. Hemakumara, P. Houston, J. Hu, M. Hua, Q. Huang, A. Huang, S. Jiang, H Kawai, D. Kinzer, M. Kuball, A. Kumar, K. B. Lee, X. Li, D. Marcon, M. März, R. McCarthy, G. Meneghesso, M. Meneghini, E. Morvan, A. Nakajima, E. M. S. Narayanan, S. Oliver, T. Palacios, D. Piedra, M. Plissonnier, R. Reddy, M. Sun, I. Thayne, A. Torres, N. Trivellin, V. Unni, M. J. Uren, M. V. Hove, D. J. Wallis, J. Wang, J. Xie, S. Yagi, S. Yang, C. Youtsey, R. Yu, E. Zanoni, S. Zeltner, Yuhao Zhang, *J. Phys. D, Appl. Phys.* **2018**, 51, 163001.

[4] H. Amano, M. Kito, K. Hiramatsu, I. Akasaki, *Jpn. J. Appl. Phys.* **1989**, 28, L2112.

[5] S. Nakamura, T. Mukai, M. Senoh, *Appl. Phys. Lett.* **1994**, 64, 1687.

[6] S. Kaneki, J. Ohira, S. Toiya, Z. Yatabe, J. T. Asubar, T. Hashizume, *Appl. Phys. Lett.* **2016**, 109, 162104.

[7] K. Nishiguchi, S. Kaneki, S. Ozaki, T. Hashizume, *Jpn. J. Appl. Phys.* **2017**, 56, 101001.

[8] T. Oka, T. Ina, Y. Ueno, J. Nishi, *Appl. Phys. Express* **2015**, 8, 054101.

[9] D. Ji, A. Agwal, H. Li, W. Li, S. Keller, S. Chowdhury, *IEEE Electron Dev. Lett.* **2018**, 39, 863.

[10] D. Ji, W. Li, A. Agwal, S. H. Chan, J. Haller, D. Bisi, M. Labrecque, C. Gupta, B. Cruse, R. Lal, S. Keller, U. K. Mishra, S. Chowdhury, *IEEE Electron Dev. Lett.* **2018**, 39, 1030.

[11] B. N. Feigelson, T. J. Anderson, M. Abraham, J. A. Freitas, J. K. Hite, C. R. Eddy, F. J. Kub, *J. Cryst. Growth* **2012**, 350, 21.

[12] T. J. Anderson, B. N. Feigelson, F. J. Kub, M. J. Tadjer, K. D. Hobart, M. A. Mastro, J. K. Hite, C. R. Eddy, *Electron. Lett.* **2014**, 50, 197.

[13] J. D. Greenlee, T. J. Anderson, B. N. Feigelson, K. D. Hobart, F. J. Kub, *Phys. Status Solidi* A **2015**, 212, 2772.

[14] T. J. Anderson, J. D. Greenlee, B. N. Feigelson, J. K. Hite, K. D. Hobart, F. J. Kub, *IEEE Trans. Semicond. Manuf.* **2016**, 29, 343.

[15] K. Nomoto, K. Takahashi, T. Oikawa, H. Ogawa, T. Nishimura, T. Mishima, H. G. Xing, T. Nakamura, *ECS Trans.* **2015**, 69, 105.

[16] T. Oikawa, Y. Saijo, S. Kato, T. Mishima, T. Nakamura, Nuclear Instruments, *Methods in Physics Research B* **2015**, 365, 168.

[17] T. Narita, T. Kachi, K. Kataoka, T. Uesugi, *Appl. Phys. Exp.* **2017**, 10, 016501.

[18] T. Niwa, T. Fujii, T. Oka, *Appl. Phys. Express* **2017**, 10, 091002.

[19] I. Akasaki, H. Amano, M. Kito, K. Hiramatsu, *J. Lumin.* **1991**, 48 & 49, 666.

[20] T. Tanaka, A. Watanabe, H. Amano, Y. Kobayashi, I. Akasaki, S. Yamazaki, M. Koike, *Appl. Phys. Lett.* **1994**, 65, 593.

[21] W. Götz, N. M. Johnson, J. Walker, D. P. Bour, R. A. Street, *Appl. Phys. Lett.* **1996**, 68, 667.

[22] A. Uedono, S. Takashima, M. Edo, K. Ueno, H. Matsuyama, H. Kudo, H. Naramoto, S. Ishibashi, *Phys. Status Solidi B* **2015**, 252, 2794.

[23] A. Uedono, S. Takashima, M. Edo, K. Ueno, H. Matsuyama, W. Egger, T. Koschine, C. Hugenschmidt, M. Dickmann, K. Kojima, S.F. Chichibu, S. Ishibashi, *Phys. Status Solidi B* **2018**, 255, 1700521.

[24] M. Akazawa, N. Yokota, K. Uetake, *AIP Advances* **2018**, 8, 025310.

[25] G. Alfieri, V.K. Sundaramoorthy, R. Micheletto, *J. Appl. Phys.* **2018**, 123, 205303.

[26] M. Akazawa, K. Uetake, *Jpn. J. Appl. Phys.* **2019**, 58, SCCB10.

[27] P. Kamyczek, E. Placzek-Popko, E. Zielony, Z. Zytkiewicz, *Material Science-Poland* **2013**, 31, 572.

[28] P. Hacke, T. Detchprohm, K. Hiramatsu, N. Sawaki, K. Tadatomo, K. Miyake, *J. Appl. Phys.* **1994**, 76, 304.

[29] E. H. Nicollian, J. R. Brews, *MOS (Metal Oxide Semiconductor) Physics and Technology*, Wiley, Hoboken, NJ, USA **2003**, Ch. 5.

[30] W. A. Hill, C. C. Coleman, *Solid-State Electronics* **1980**, 23, 987.

[31] S. M. Sze, K. K. Ng, *Physics of Semiconductor Devices*, 3rd edn, Wiley, Hoboken, NJ, USA **2007**, Ch. 4.

[32] K. S. Cole, R. H. Cole, *J. Chem. Phys.* **1941**, 9, 341.

[33] T. Sawada, H. Hasegawa, *Phys. Status Solidi A* **1979**, 54, 689.

[34] H. Hasegawa, H. Ohno, *J. Vac. Sci. & Technol. B* **1986**, 4, 1130.

[35] H. Hasegawa, M. Akazawa, *Appl. Surf. Sci* **2008**, 254, 8005.

[36] U. Honda, Y. Yamada, Y. Tokuda, K. Shiojima, *Jpn. J. Appl. Phys.* **2012**, 51, 04DF04.

[37] Z.-Q. Fang, D. C. Look, W. Kim, Z. Fan, A. Botchkarev, H. Morkoç, *Appl. Phys. Lett.*

1998, 72, 2277.

[38] Z.-Q. Fang, D. C. Look, X.-L. Wang, J. Han, F. A. Khan, I. Adesida, *Appl. Phys. Lett.* **2003**, 82, 1562.

[39] Z.-Q. Fang, D. C. Look, D. H. Kim, I. Adesida, *Appl. Phys. Lett.* **2005**, 87, 182115.

[40] Y. Tokuda, Y. Matsuoka, H. Ueda, O. Ishigro, N. Soejima, T. Kachi, *Superlattice and Microstructures* **2006**, 40, 268.

[41] J. L. Lyons, C. G. Van de Walle, *NPJ Computational Materials* **2017**, 12, 1.

[42] H. J. von Bardeleben, J. L. Cantin, U. Gerstmann, A. Scholle, S. Greulich-Weber, E. Rauls, M. Landmann, W. G. Schmidt, A. Gentils, J. Botsoa, M. F. Barthe, *Phys. Rev. Lett.* **2012**, 109, 206402.

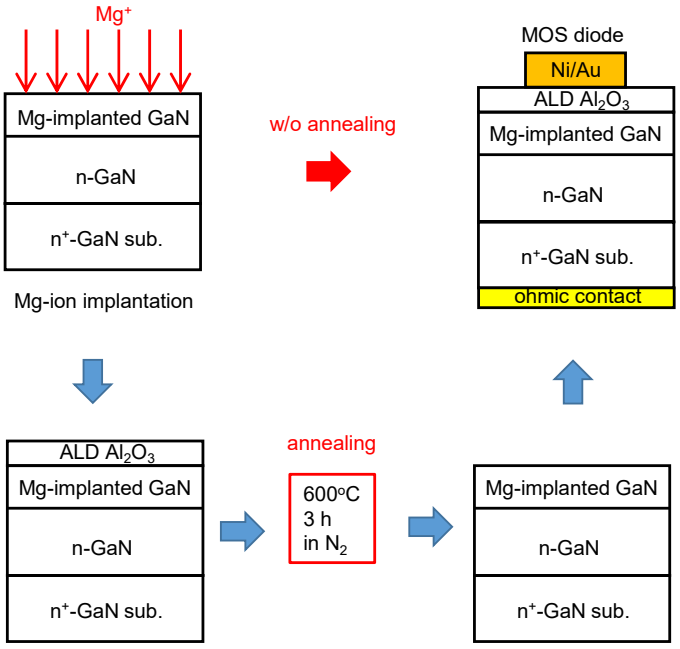


Figure 1. Fabrication sequence for tested GaN MOS diodes.

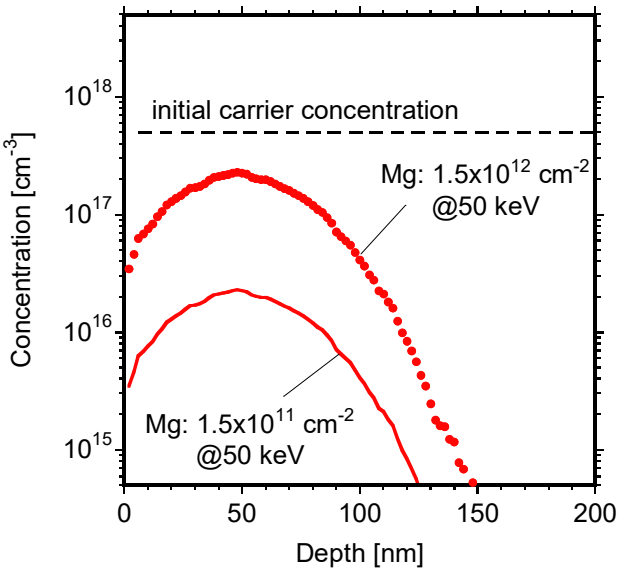


Figure 2. TRIM simulation results of Mg concentration in GaN for two cases of Mg-ion implantation with different dosages.

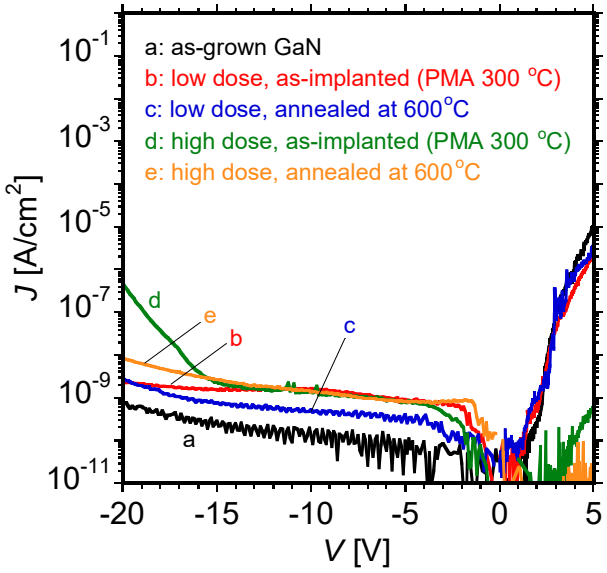


Figure 3. Summary of *J*–*V* characteristics measured for all samples.

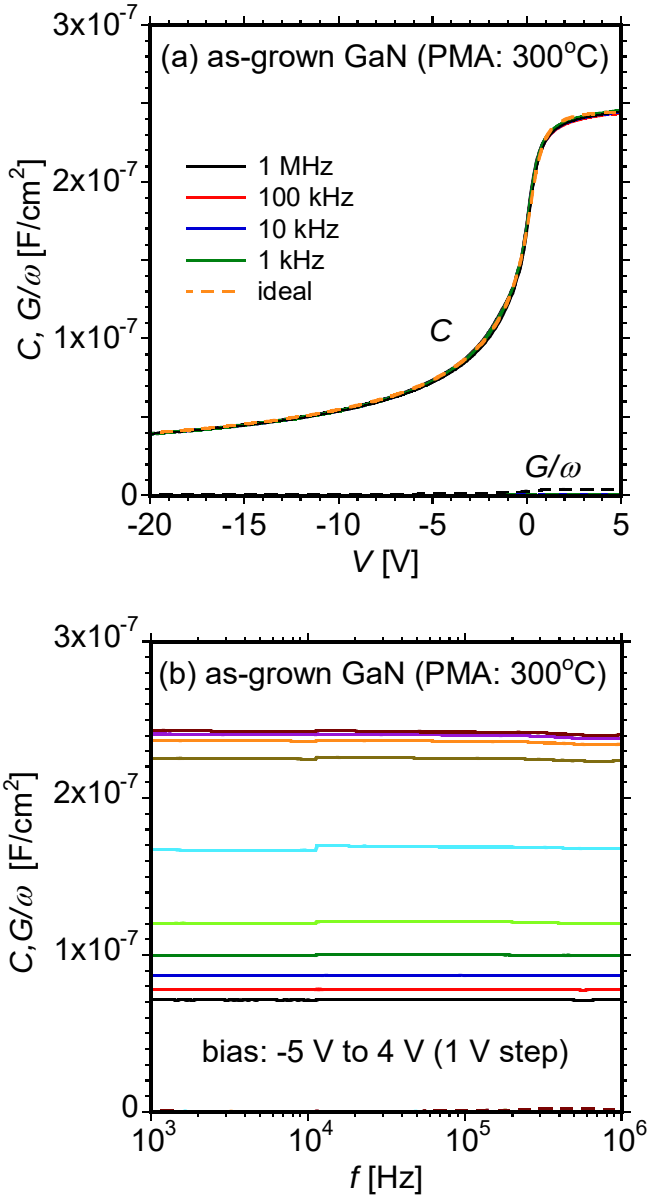


Figure 4. (a) *C–V* and (b) *C–f* characteristics for the MOS diode with as-grown GaN without Mg-ion implantation.

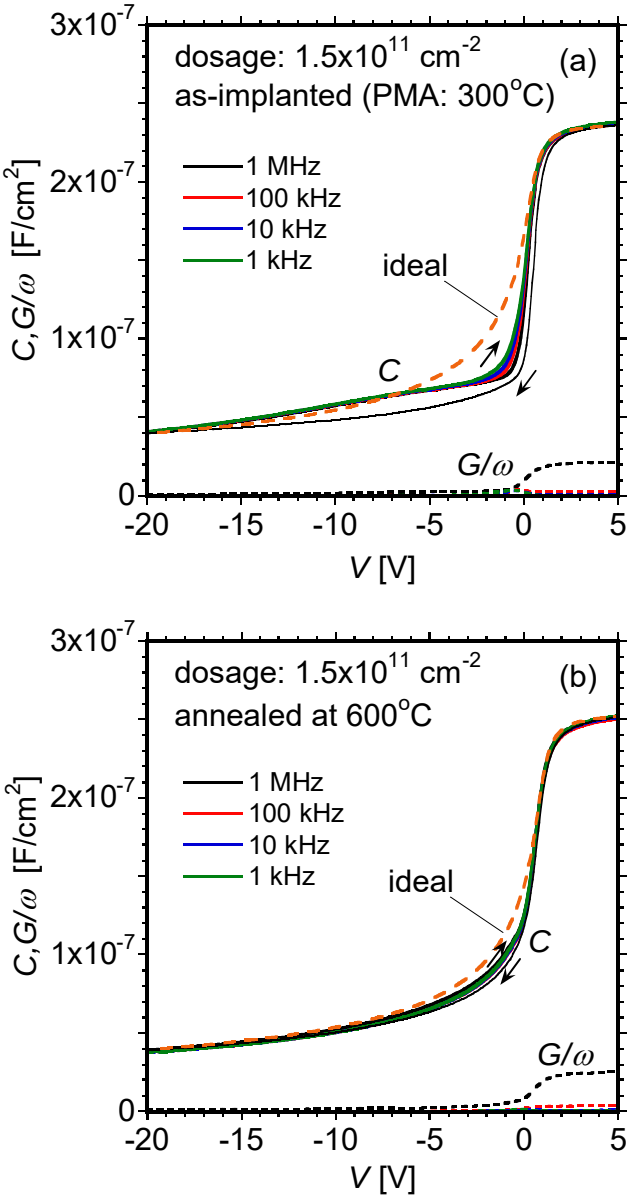


Figure 5. *C–V* characteristics for the low-dosage sample: (a) without and (b) with 600 °C annealing.

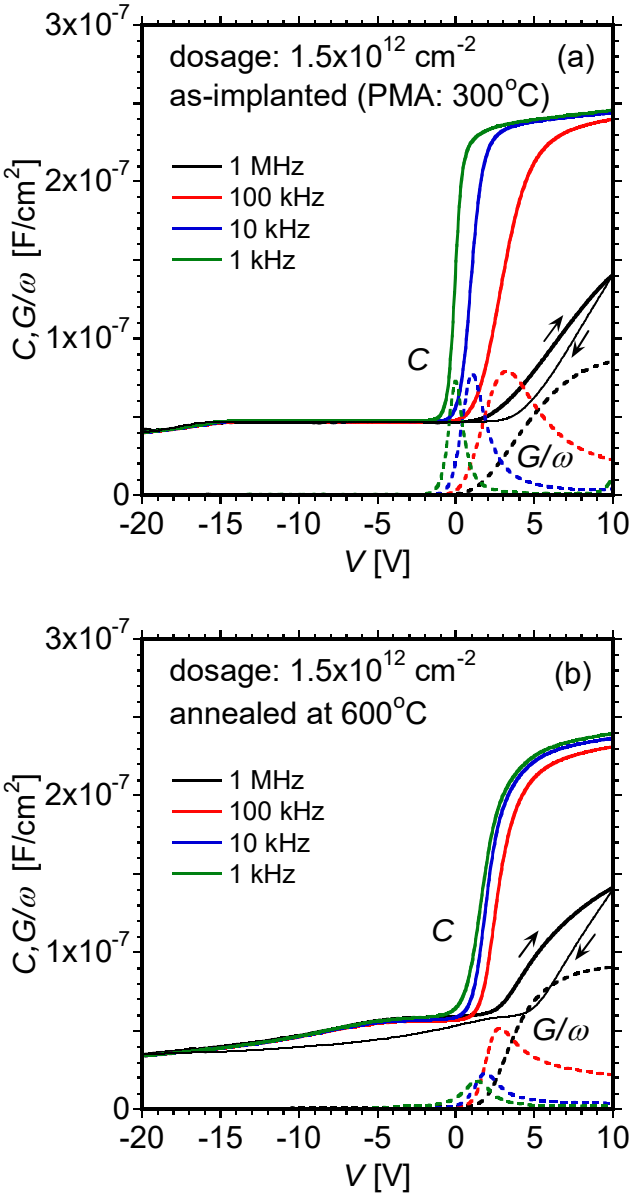


Figure 6. *C–V* characteristics for the high-dosage sample: (a) without and (b) with 600 °C annealing.

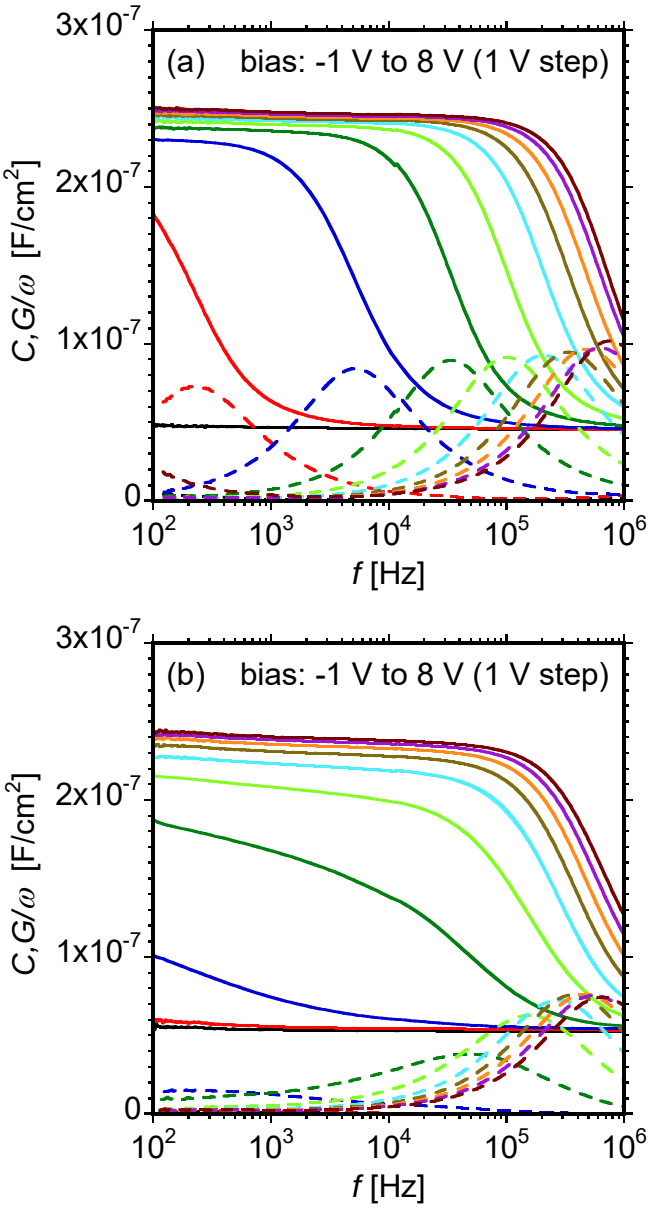


Figure 7. *C–f* characteristics for the higher dosage sample: (a) without and (b) with 600 °C annealing.

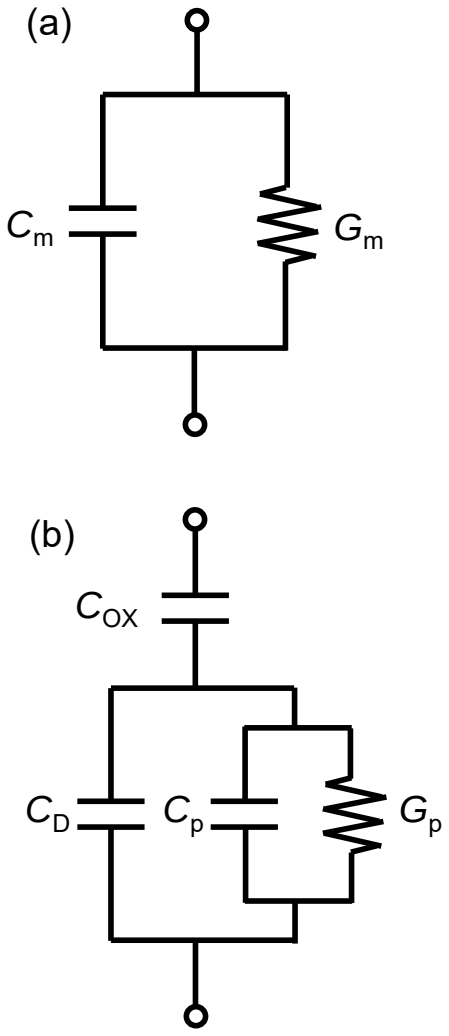


Figure 8. Equivalent circuits. (a) Circuit for measurement data. (b) Circuit for physical model of MOS diode including interface trap admittance.

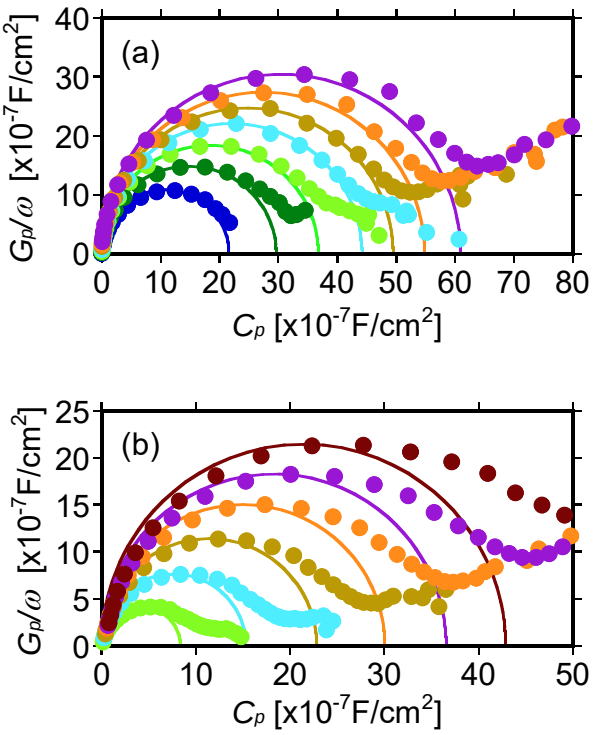


Figure 9. Cole–Cole diagrams for the high-dosage sample: (a) without and (b) with 600 ºC annealing. The solid lines are fitting lines using Equation (6).

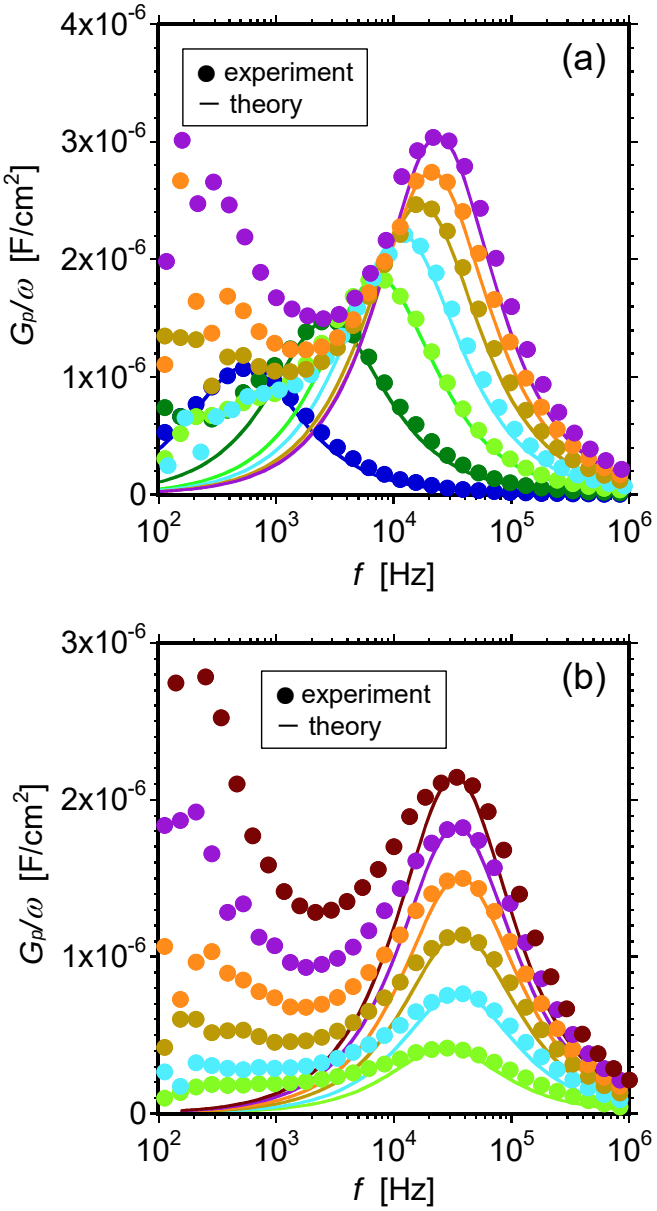


Figure 10. Calculated G_p/ω for the high-dosage sample: (a) without and (b) with 600 ºC annealing. The solid lines are fitting lines using Equation (5).

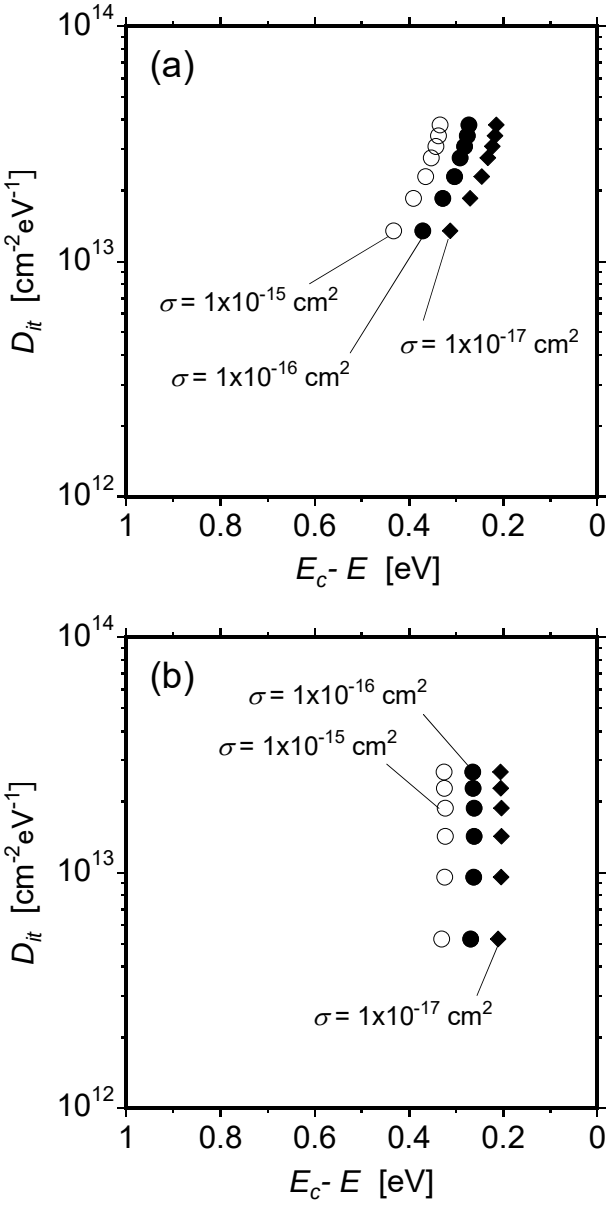


Figure 11. Calculated D_{it} distributions for the high-dosage sample with three different σ: (a) without and (b) with 600 °C annealing.

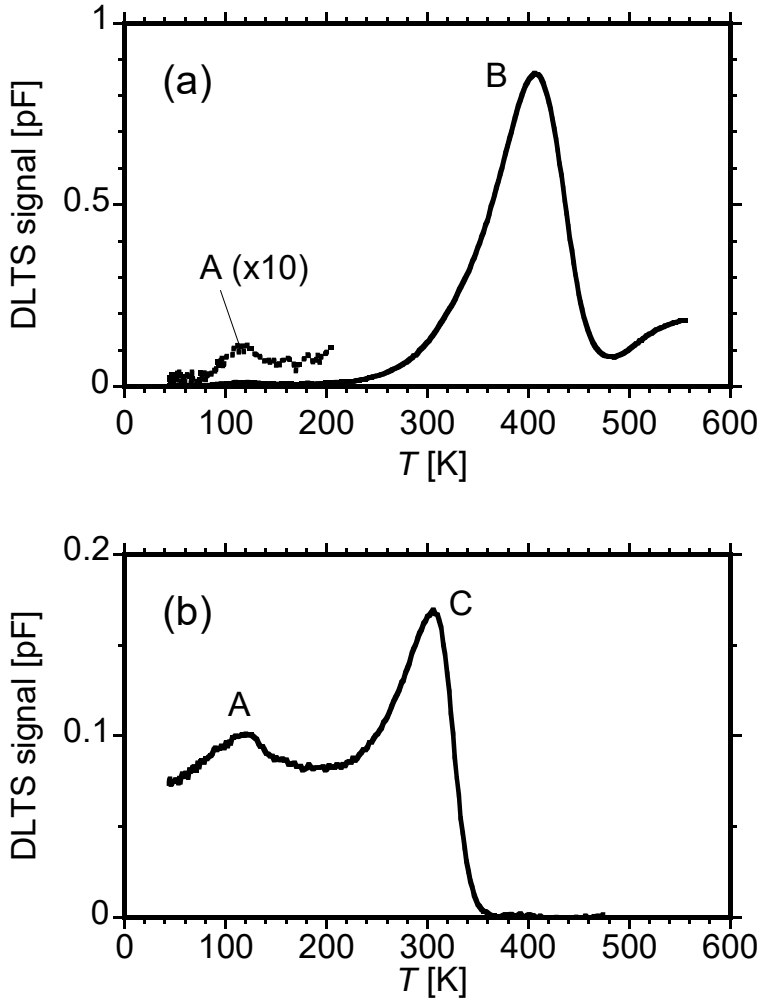


Figure 12. DLTS signals obtained for (a) the low-dosage sample and (b) the high-dosage sample.

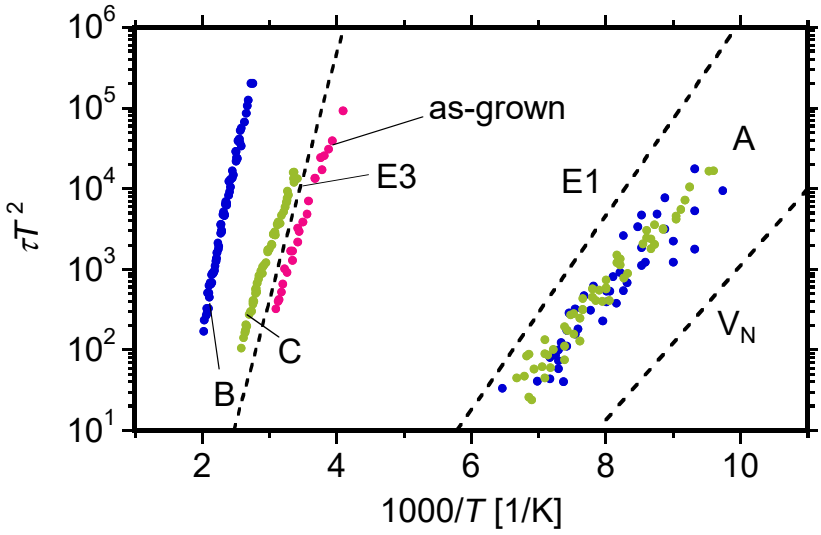


Figure 13. Arrhenius plots of detected deep levels.